Integrated Geological and Petrophysical Approaches for Characterizing the Pre-Cenomanian Nubian Sandstone Reservoirs in Ramadan Oil Field, Central Gulf of Suez, Egypt

Ahmed H. Saleh[1] · Wafaa A. El Hemimey[1] · Mahmoud Leila[2]

Abstract

The present study integrates multidisciplinary geological and petrophysical approaches to characterize and evaluate the potential of the pre-Cenomanian Nubian sandstone reservoirs in the Ramadan oil field, the central offshore part of the Gulf of Suez, Egypt. The different petrophysical parameters of the Nubian sandstone reservoirs (shale volume, porosity, water saturation as well as gross and net-pay thicknesses) were mapped, and 3D slicing models for the hydrocarbon phases saturation were constructed to understand the reservoir heterogeneity and the distribution of the best reservoir facies. The petrophysical results of the pre-Cenomanian Nubian succession highlight very good reservoir intervals in the Nubian C sandstones containing thick pay zones (> 120 m). On the other side, the Nubian A and B reservoir rocks are less prospective with pay zone horizons (< 10 m). Integrated reservoir models and wireline log analysis elucidate that clay volume is the most detrimental factor to the reservoir quality as the pay zone thickness and hydrocarbon saturation often increase where the clay volume decreases. Therefore, the presence of scattered pay zone intervals in Nubian A and B is mainly related to their elevated clay content which acts as barriers for fluids flowing within the reservoir facies. The Nubian C succession contains three different reservoir rock types (RRT) with variable compositional and petrophysical properties. RRTI and RRTII sandstones comprise quartzose sandstones with very low clay content (< 10%) and are characterized by an open pore system dominated by macropores. These sandstones are less impacted by overburden pressure and therefore can preserve their depositional porosity and permeability. On the other hand, RRTIII reservoir rocks are clay rich (> 10%) with abundant mesopores that are more prone to compressibility and hence reduction of the pore volume and pore throat. The present study highlights the significance of comprehensive integration between wireline logs, cores, and 3D reservoir models in directing exploration endeavors toward prospective reservoirs in mature basins.

Keywords 3D reservoir slicing · Petrophysical rock typing · Wireline logging · Core analysis · Clastic reservoirs

1 Introduction

Understanding the distribution of potential reservoir facies and the spatiotemporal evolution of the reservoir porosity–permeability characteristics is essential for reservoir management, development, and prospect evaluation in petroliferous basins [1–5]. A comprehensive integration between multidisciplinary geological and petrophysical approaches

✉ Ahmed H. Saleh
  Ahmohammed@zu.edu.eg

1 Geology Department, Faculty of Science, Zagazig University, Zagazig, Egypt

2 Geology Department, Faculty of Science, Mansoura University, Mansoura, Egypt
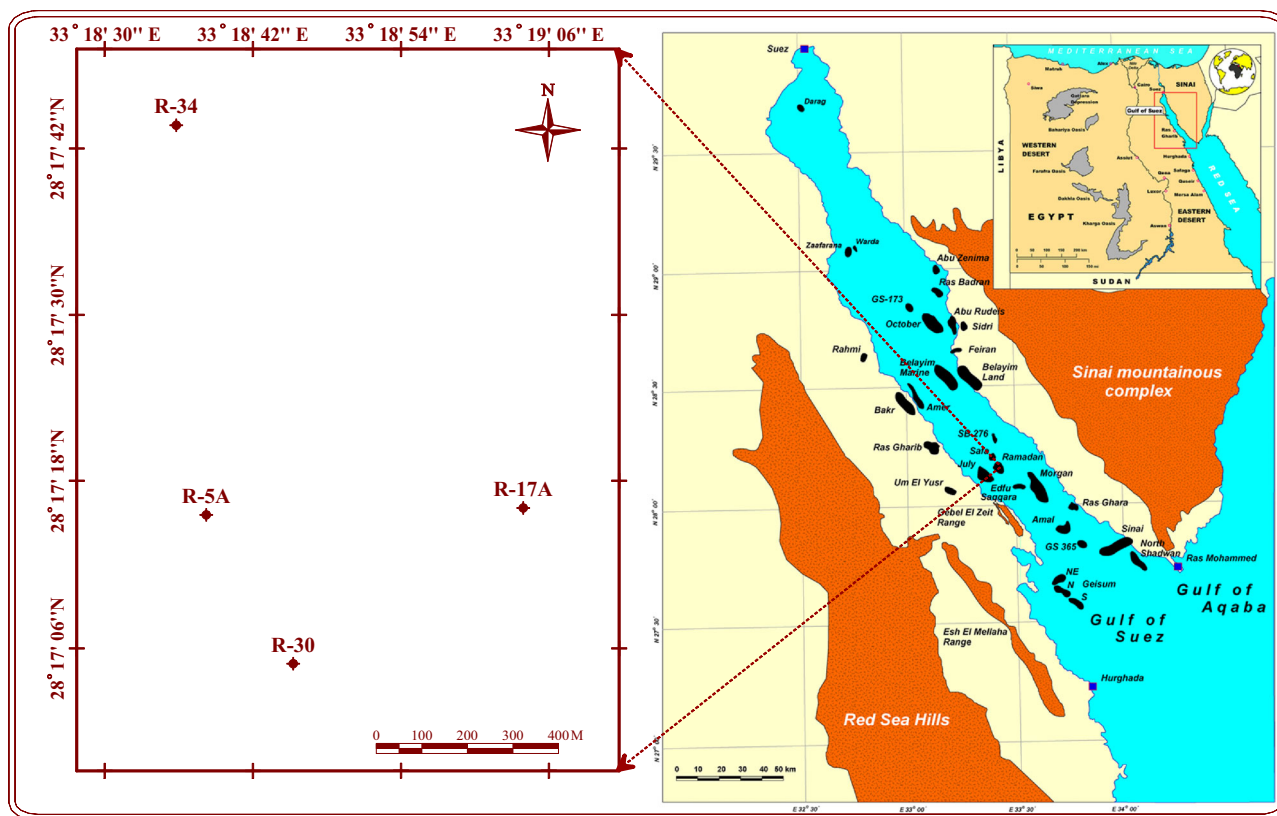
is crucial for a high-resolution determination of the reservoir pore volume and the potential reservoir rock types [3, 6–11]. The pre-Cenomanian Nubian sandstone represents the principal reservoir target in the pre-rift sedimentary succession in the Gulf of Suez producing crude oil from several oil fields in the Gulf of Suez (e.g., Ramadan, July, Ras Gharib, Hurghada, Sidki, and October) [12–14]. Published studies on the pre- and syn-rift facies were focused on their hydrocarbon potentiality [14–16] and tectono-stratigraphic evolution [17–19]. The reservoir characteristics of the pre-rift succession were also delineated in several fields [13]. However, a detailed rock typing for the pre-Cenomanian reservoirs is still poorly constrained. Moreover, a comprehensive assessment for the pre-Cenomanian reservoir facies heterogeneity and understanding the link between their matrix composition and pore

Fig. 1 Location map illustrating the main oil-producing fields in the Gulf of Suez, Egypt, with focus on the studied Ramadan oil field wells [15]

system characteristics are crucial for hydrocarbon exploration campaign in the Gulf of Suez. Matrix composition of clastic reservoirs controls has a paramount influence on their reservoir quality. For example, coarse-grained quartzose sandstones commonly have a more connected pore system than clay-rich and cement-rich facies [2–5]. Additionally, some specific mineral phases (e.g., ductile framework components) are detrimental to the reservoir characteristics as they commonly reduce in the pore spaces after compaction and thereby destroying the primary intergranular porosity [1–4]. The present study aims at evaluating the potentiality of the pre-rift Nubian sandstone reservoir in the Ramadan oil field (Fig. 1) as well as understanding the factors controlling their heterogeneity and distribution of the best reservoir facies. Ramadan oil field represents one of the major oil-producing fields in the Gulf of Suez hosting several hundred million barrels of proven oil reserves, thus ranking it as the fourth largest oil field in Egypt [14].

Gulf of Suez represents a highly deformed rift basin at the boundary of the African and Arabian plates containing very petroliferous pre- and syn-rift sedimentary successions hosting potential source rock and reservoir intervals (Fig. 2) [16–19]. The pre-Cenomanian Nubian siliciclastic sedimentary successions host very promising reservoir targets ranging in age from Cretaceous to Cambrian-Ordovician [20, 21]. The Nubian successions in the Gulf of Suez are classified from older to younger into the following groups, and formations: Qebliat Group, Umm Bogma Formation, Ataqa Group, and El-Tih Group, which are equivalent to the Nubian D, C, B, and A units, respectively (Fig. 2) [22–24]). The Nubian A, C, and D units consist mainly of sandstones with minor shale interbeds, whereas the Nubian B comprises interbedded sandstone and shale with minor carbonate facies (Fig. 2).

The reservoir Nubian sedimentary succession accumulated mainly in fluvial and shallow marine depositional environments. The Nubian sandstones consist mainly of mature quartz arenite with very good reservoir quality; however, the porosity–permeability characteristics of the Nubian clastics vary greatly from Nubian D to A units [25]. The Nubian C unit represents the principal reservoir target in many producing fields in the Gulf of Suez such as the Ramadan and July oil fields [22]. The studied wells in the Ramadan oil field encounter a net-pay thickness in Nubian C sandstone of approximately 310 m. This great thickness of the hydrocarbon column typifies very potential reservoir characteristics of these sandstone beds. Therefore, a high-resolution investigation of the Nubian sandstone reservoir target and detailed analyses of their poro-perm characteristics and distribution of the best reservoir facies are crucial for the petroleum exploration and development campaign in the Gulf of Suez.
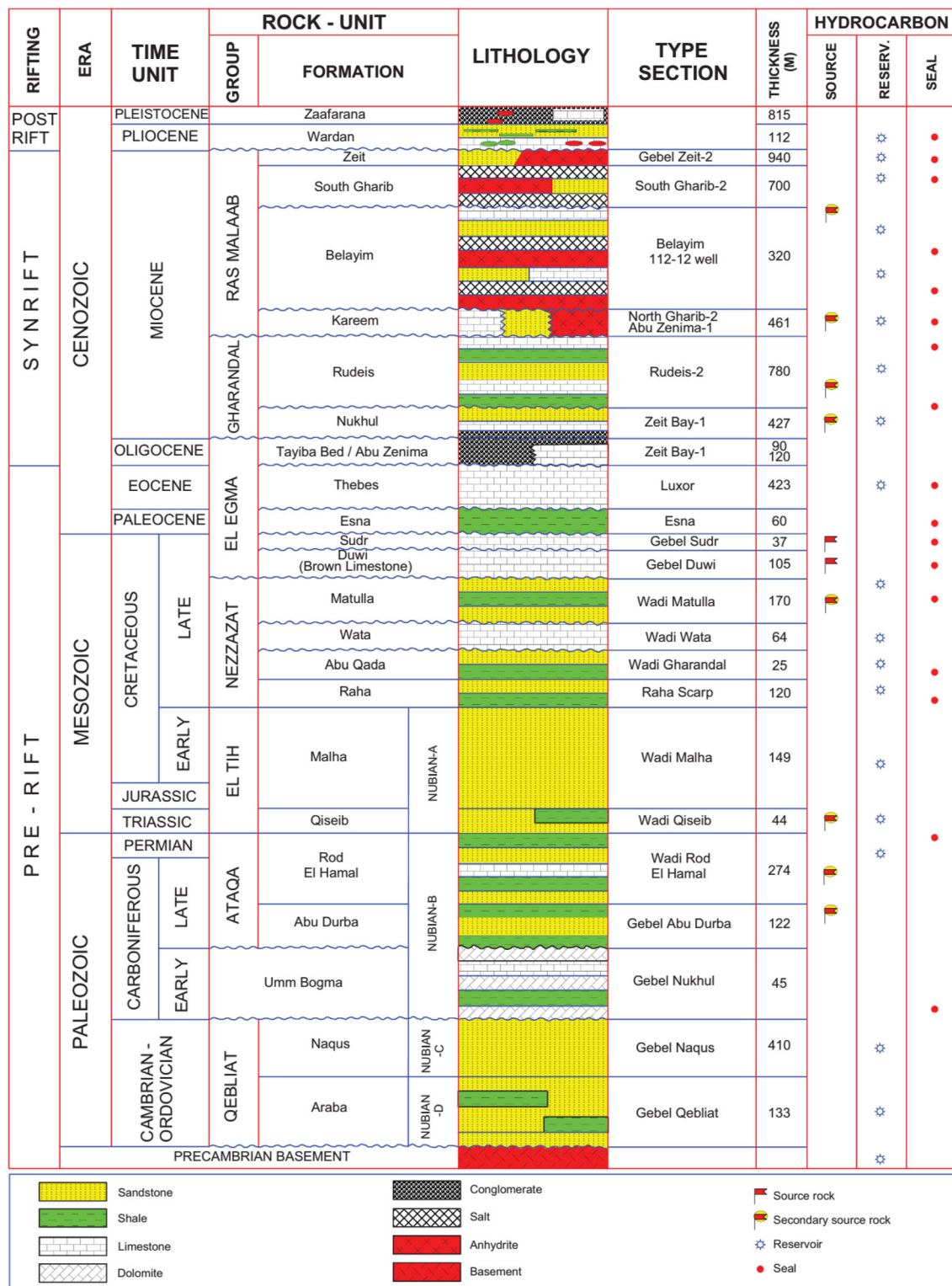
| RIFTING | ERA | TIME UNIT | | ROCK - UNIT | | LITHOLOGY | TYPE SECTION | THICKNESS (M) | HYDROCARBON | | |
			GROUP	FORMATION					SOURCE	RESERV.	SEAL
POST RIFT	CENOZOIC	PLEISTOCENE			Zaafarana			815			
		PLIOCENE			Wardan			112		✿	●
SYNRIFT		MIOCENE	RAS MALAAB		Zeit		Gebel Zeit-2	940		✿	●
					South Gharib		South Gharib-2	700	⚑	✿	●
					Belayim		Belayim 112-12 well	320		✿ / ✿	● / ●
			GHARANDAL		Kareem		North Gharib-2 Abu Zenima-1	461	⚑	✿	● / ●
					Rudeis		Rudeis-2	780	⚑	✿	●
					Nukhul		Zeit Bay-1	427	⚑	✿	●
PRE - RIFT		OLIGOCENE	EL EGMA		Tayiba Bed / Abu Zenima		Zeit Bay-1	90 / 120			
		EOCENE			Thebes		Luxor	423		✿	●
		PALEOCENE			Esna		Esna	60			●
	MESOZOIC				Sudr		Gebel Sudr	37	⚑		●
					Duwi (Brown Limestone)		Gebel Duwi	105	⚑	✿	●
		CRETACEOUS LATE	NEZZAZAT		Matulla		Wadi Matulla	170	⚑		●
					Wata		Wadi Wata	64		✿	
					Abu Qada		Wadi Gharandal	25		✿	●
					Raha		Raha Scarp	120		✿	●
		CRETACEOUS EARLY	EL TIH	NUBIAN-A	Malha		Wadi Malha	149		✿	
		JURASSIC									
		TRIASSIC			Qiseib		Wadi Qiseib	44	⚑	✿	●
	PALEOZOIC	PERMIAN	ATAQA	NUBIAN-B	Rod El Hamal		Wadi Rod El Hamal	274	⚑	✿	
		CARBONIFEROUS LATE			Abu Durba		Gebel Abu Durba	122	⚑		
		CARBONIFEROUS EARLY			Umm Bogma		Gebel Nukhul	45			●
		CAMBRIAN - ORDOVICIAN	QEBLIAT	NUBIAN-C	Naqus		Gebel Naqus	410		✿	
				NUBIAN-D	Araba		Gebel Qebliat	133		✿	
		PRECAMBRIAN BASEMENT								✿	

Legend:
- Sandstone (yellow)
- Shale (green)
- Limestone
- Dolomite
- Conglomerate
- Salt
- Anhydrite
- Basement
- ⚑ Source rock
- ⚑ Secondary source rock
- ✿ Reservoir
- ● Seal

Fig. 2 Generalized lithostratigraphic column of the Gulf of Suez illustrating the studied stratigraphic intervals [23, 24]

2 Geologic Setting

The Gulf of Suez is a complex rift system consisting of three different segments with variable fault throws and fault-related structures (Fig. 3). The Gulf of Suez rift segments are separated by NE-SW accommodation transform zones [26–28]. These segments from north to south include the Darag basin with SW-dipping half-graben structures, the Belayim province containing NE-dipping half grabens, and the Amal-Zeit province with SW-dipping half-graben (Fig. 3). The rift segments are separated by the Galala-Abu Zenima (ZAZ) and Morgan accommodation zones. The Gulf of Suez contains rock units that range in age from Precambrian to recent (Fig. 2). The lithostratigraphy of the Gulf of Suez is subdivided into three lithostratigraphic mega sequences including the pre-rift, syn-rift, and post-rift successions [23, 29, 30]. The pre-rift successions range in age from Precambrian to Eocene; the syn-rift includes the Oligocene–Miocene successions, whereas the post-rift successions comprise the post-Miocene facies. These successions vary greatly in thickness, facies, and architecture from one segment to another ([23, 26, 31–33] and references therein). Several active petroleum systems have been reported where the rift-faults are the main migration paths for the expelled oil from the pre-rift Cretaceous (e.g., Duwi limestone) and post-rift Miocene source rocks to the clastic

Fig. 3 A geologic map illustrates the three main structural provinces and the different structural patterns affecting the Gulf of Suez [31]
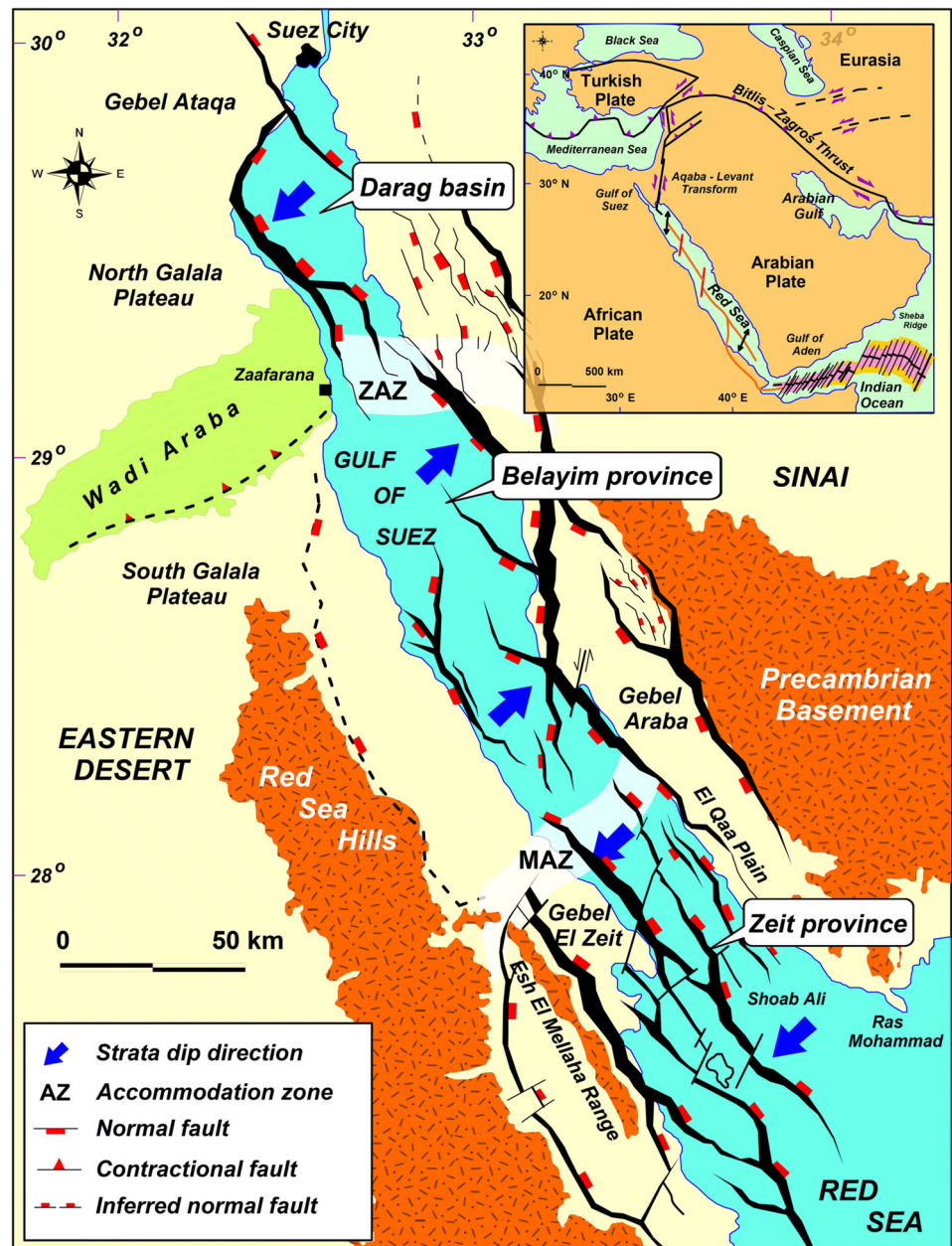
reservoir facies [16–18]. The pre-rift clastic Nubian reservoirs were likely charged from the Cretaceous source rocks [23]. However, variation in oil signature (oil families) in the Gulf of Suez reservoirs is due to the presence of several active source rocks such as the Duwi limestone, Esna, and Nukhul formations [15].

The Nubian siliciclastic intervals present the most prolific pre-rift sedimentary successions in the Gulf of Suez segments. The Nubian siliciclastics range in age from Paleozoic to Early Cretaceous. They rest unconformably on the Precambrian basement complex [23, 34]. The Nubian siliciclastic rocks comprise four members having different ages and depositional facies. These are the Nubian D and C (Early Paleozoic), Nubian B (Carboniferous-Permian), and Nubian A (Early Cretaceous) [19, 35, 36]. The Lower Paleozoic Nubian siliciclastic rocks (Qebliat Group) are distributed over the whole Gulf of Suez and represent the oldest regressive marine facies. The Qebliat Group is divided into two formations, Araba and Naqus formations that are thickening northward [23, 35, 37–39]. The Araba Formation is equivalent to the informal Nubian (D); it consists of interbedded fine- to medium-grained, colorless to yellowish-white sandstones and gray to greenish-gray mudstones. On the other hand, Naqus Formation is a continental sequence of thick, massive, pebbly, cross-bedded sandstones with minor clay interbeds. The formation is Ordovician in age and is equivalent to the Nubian (C). The Carboniferous Nubian clastics comprise shallow marine sandstones and siltstones interbedded with fossiliferous black shales and mudstones [35, 38]. Moreover, the Mesozoic Nubian clastics consist of white to pale yellow clean quartzose, cross-bedded fluvial, and shallow marine sandstones with minor carbonate intercalations [40, 41].

3 Data and Methods

3.1 Wireline Logging

The present study is based on a complete subsurface dataset including wireline logs and cores from four wells (R-34, R-5A, R-17A, and R-30) in the Ramadan oil field (Fig. 1). The wireline logs comprise gamma ray, caliper, density, shallow and deep resistivity, neutron, sonic, and the photoelectric factor (Fig. 3). The wireline logs were interpreted using Schlumberger Techlog software to evaluate the reservoir potential of the pre-Cenomanian Nubian clastics in the studied wells. The deduced reservoir parameters include reservoir gross thickness, shale volume (Vsh), total and effective porosity (PhiT, PhiE), water saturation (Sw), bulk pore volume (BPV), net-pay thickness (N.P.Th), and hydrocarbon saturation (Sh) as well as the oil in place indicator (OIPI) (Fig. 4). The wireline logging analyses were applied

using the standard interpretation procedures of Poupon and Leveaux [42] and Asquith and Gibson [43]. The neutron—density cross-plot was utilized to determine porosity as well as the matrix characteristics using the interpretation charts of Schlumberger [44]. The neutron, sonic, and density logs have been integrated to determine the cementation and saturation exponents (M and N) which are dependent on porosity [44, 45]. 3-D reservoir slicing in the three directions (Easting, Northing, and Depth) or (X, Y, and Z) was constructed using Tecplot software for the 3D visualization of variations in the distribution of the pre-Cenomanian Nubian sandstone reservoir parameters. For this, the values of each reservoir parameter were contoured horizontally then vertical contouring was constructed in order to elicit the values between the different reservoir intervals. The 3D contour values were calculated at the interpolation nodes $x_1, x_2, \cdots, x_n$ using the linear equation of Davis [46]:

$$F(x) = ((x_2 - x)f(x_1) + (x - x_1)f(x_2)) / (x_2 - x_1).$$

3.2 Conventional and Special Core Analyses

Conventional core analyses (CCA) were performed on 51 cylindrical core plugs from the Nubian C interval in the R1-34 well at Corex laboratories, Egypt. The CCA involves the measurement of porosity, permeability, grain density, and water saturation. Helium porosimeter and nitrogen permeameter were utilized in order to obtain porosity and permeability values, respectively. Additionally, water saturation was measured using the distillation–extraction procedure of Dean and Stark [47]. The reservoir quality evaluation parameters such as the flow zone indicator (FZI), normalized porosity index (NPI), and reservoir quality index (RQI) were calculated as functions of porosity and permeability [6] as follows:

$$NPI = \phi / (1 - \phi)$$

$$RQI = 0.0314\sqrt{K/\phi}$$

$$FZI = RQI / NPI$$

Moreover, the average effective pore throat radius (R_{35}) values were calculated from the measured core porosity and permeability values using the Winland formula [48] as the following:

$$Log (R_{35}) = 0.732 + 0.588 \log (K) - 0.864 \log(\phi)$$

Special core analyses (SCA) were performed on 10 samples from the Nubian C interval in the R1-34 well and involve the assessment of the capillary properties as well as the
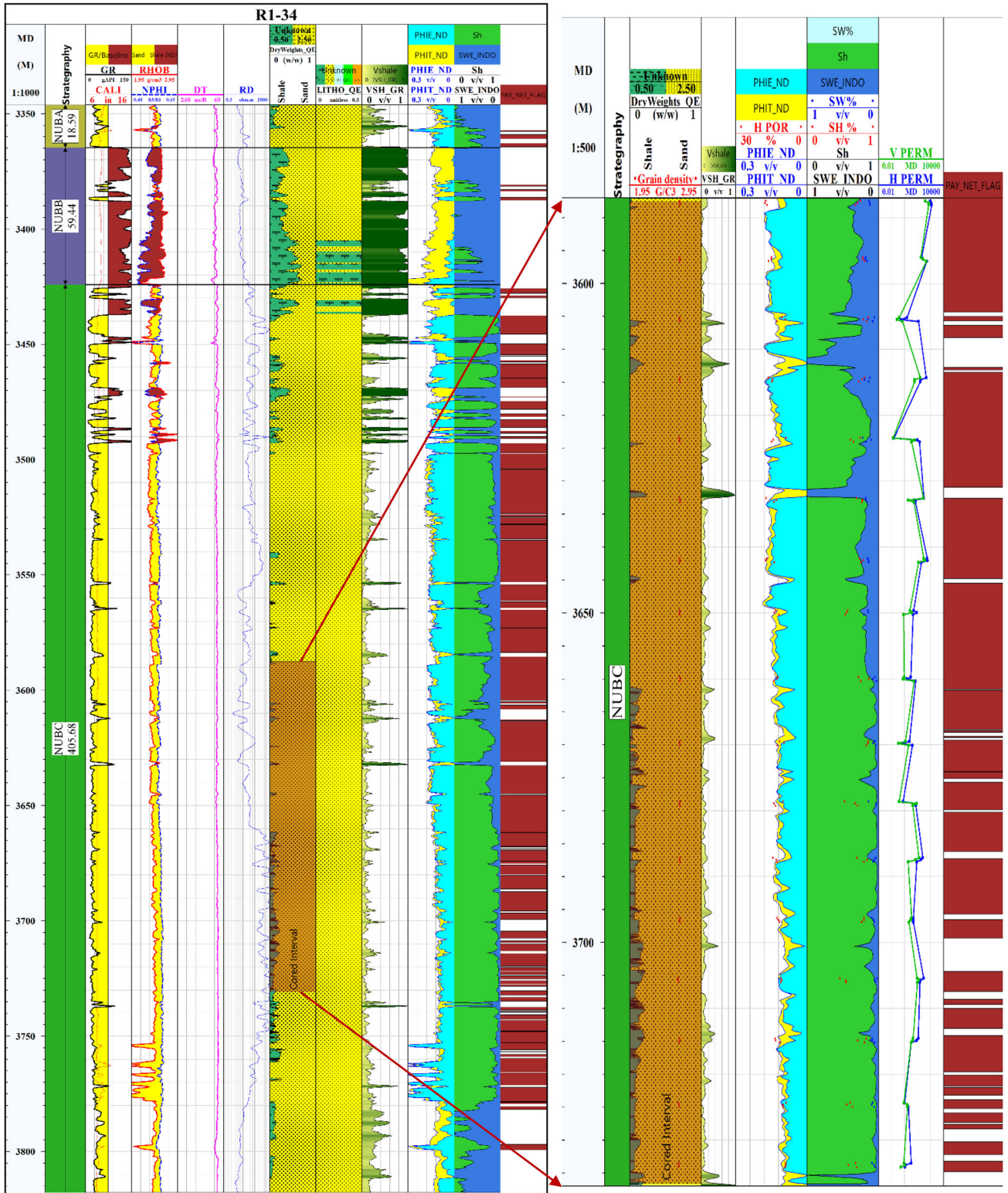
Fig. 4 Lithosaturation cross-plot with a detailed core interval showing the different petrophysical characteristics of the pre-Cenomanian Nubian successions in R1-34 well, Ramadan oil field

impact of the overburden stress on the reservoir porosity and permeability. Mercury injection capillary pressure tests (MICP) were performed according to the standard analytical procedure of Leverett [49] and Vavra et al. [50]. For MICP dry, clean samples were loaded into a mercury-filled camper. The mercury injection pressure is gradually increased, and the relation between the volume of intruded mercury inside the pore spaces and injection pressure was plotted. The impact of incremental confining pressure (from 1000 psi up to 6000 psi, with an increasing rate of 1000 psi/step) on the measured petrophysical parameters, porosity, horizontal permeability, and vertical permeability, was measured, and the pore reduction (PR) was deduced. For that, porosity and permeability were measured, and then the applied pressure was increased incrementally up to 6000 psi. The pore reduction (PR) for porosity and permeability ($PR_\emptyset$, PR_k, respectively) was calculated as follows:

$$PR_\emptyset = \emptyset - \emptyset_{500-6000}$$

$$PR_{Kh} = K_h - K_{h500-6000}$$

where $\emptyset$ and K_h are the measured porosity and horizontal permeability at ambient pressure (~ 100 psi). Both $\emptyset_{500}$ and K_{h500} are the measured porosity at the lowest confining pressure (500 psi), whereas the $\emptyset_{6000}$ and K_{h6000} are the measured porosity and permeability at the highest pressure values (6000 psi).

4 Results and Interpretations

4.1 Lithosaturation Characteristics of the Nubian Succession

The lithosaturation cross-plots of the studied wells show that the Nubian sedimentary succession consists mainly of sandstones with shale interbeds (Fig. 4). The sand/shale ratio decreases upward from the Nubian C to Nubian B and A. The Nubian C comprises stacked clean sandstone beds with low shale volume content (Av. < 10%) (Table 1). The Nubian B and A reservoir rocks consist mainly of interbedded sand and shales where the average shale volume is often greater than 10% (Table 1). The wireline log motif varies significantly from Nubian C, B, and A. The Nubian C, A successions have blocky gamma ray motifs separated by thin intervals of serrated patterns reflecting sandstone-rich facies. On the other hand, the Nubian B rocks display cylindrical gamma ray patterns with very high values with thin interbeds of blocky motifs.

The neutron–density cross-plot of the studied wells reveals the matrix composition of the studied pre-Cenomanian Nubian reservoir rocks (Fig. 5). When the matrix lithology is a binary mixture, the points will be clustered between the corresponding lithology as (quartz-lime or lime-dolomite). Moreover, the impact of hydrocarbons (hydrocarbon effect) causes the apparent porosity from the density log to increase and porosity from the neutron log to decrease, and therefore the samples would be plotted above the sandstone line [51]. On the other hand, the abundance of iron-rich clays and/or heavy minerals will result in the deviation of the samples below the dolomite line. The Nubian C rocks have a matrix composition dominated by quartzose sandstones where most of the points are clustered close to the quartz line. Moreover, the hydrocarbon effect is more prominent in the Nubian C sandstones as they host the main hydrocarbon-bearing intervals. The plot also reveals the porosity range of Nubian C sandstones from 5 to 20%. Similarly, the Nubian B rocks are plotted below the dolomite line reflecting abundant clay-rich composition. Analog to Nubian C, the Nubian A rocks are plotted above the sandstone line reflecting the impact of hydrocarbons with a dominant sand-rich lithology.

The matrix characteristics can also be deduced from the (M–N) cross-plot. This cross-plot is used to identify the different mineral phases and their relative contents in the matrix [44, 45]. The highest M and N values are reported in the Nubian C reservoir rocks, whereas the lowest values are observed in Nubian B (Fig. 6). The M–N values reveal that the Nubian C are mainly quartzose with minimal contents of clay and/or carbonate cement. Similarly, the Nubian A reservoir rocks display M–N values reflecting their quartz-rich composition, however, the carbonate cement is more prominent in Nubian A than in Nubian C. On the other hand, the Nubian B rocks have a clay-rich lithology with minimal content of quartz sandstones. The Nubian B rocks displaying low M–N values are likely enriched in iron-rich clays (e.g., chlorite and smectite).

4.2 Isoparametric Maps and Lateral Distribution of the Petrophysical Parameters

The different petrophysical parameters deduced from wireline logging interpretation for Nubian C, B, and A reservoir rocks are presented in Table 1. The petrophysical properties vary significantly between the studied Nubian rocks. The Nubian C reservoir rocks host the greatest bulk pore volume (BPV) ranging between 20 and 42 m³ (Table 1), and the highest values of BPV are observed in the eastern part of the study region in the R5-17A well. Similarly, the initial oil in place indicator (OIPI) is higher in Nubian C member with values in the range of 17 and 39 m³ (Table 1). Notably, the BPV and OIPI values in Nubian C are at least tenfold greater than that

Table 1 The values of petrophysical parameters for Nubia A, B and C reservoir in Ramadan oil field, Central Gulf of Suez, Egypt

Member	Well	Gross (m)	Net Pay (m)	PHIT (%)	PHIE, (%)	Vsh (%)	Sw, (%)	Sh, (%)	BPV (m³)	OIPI (m³)
Nubian A	R1-34	18.29	5	16	14.6	9.9	34.2	65.8	0.7	0.45
	R5-17A	27	3.5	17.1	15.8	8.1	35.7	64.3	0.6	0.36
	R5-5A	15	0.012	15.2	11.4	12.5	94.6	5.4	0.5	0.02
	R5-30	20.82	6	23.9	20.3	12	25.5	74.5	1.2	0.91
Nubian B	R1-34	58.20	1.5	12.4	11	9.2	36.6	63.4	0.2	0.10
	R5-17A	79.5	4.7	18.6	16.7	9.7	6.6	93.4	0.8	0.73
	R5-5A	71.95	4	18.7	16.8	10.3	36.8	63.2	0.7	0.42
	R5-30	57.16	0.75	25.8	23.8	13	1.9	98.1	0.2	0.17
Nubian C	R1-34	390	202	15.9	14.3	9	19.6	80.4	28.9	23.17
	R5-17A	391	308	14.6	13.6	4.6	6.6	93.4	42	39.20
	R5-5A	226.68	131	14.6	13.6	3.9	5.3	94.7	17.8	16.90
	R5-30	245	129.5	16.6	15.3	5.8	16.3	83.7	19.8	16.58
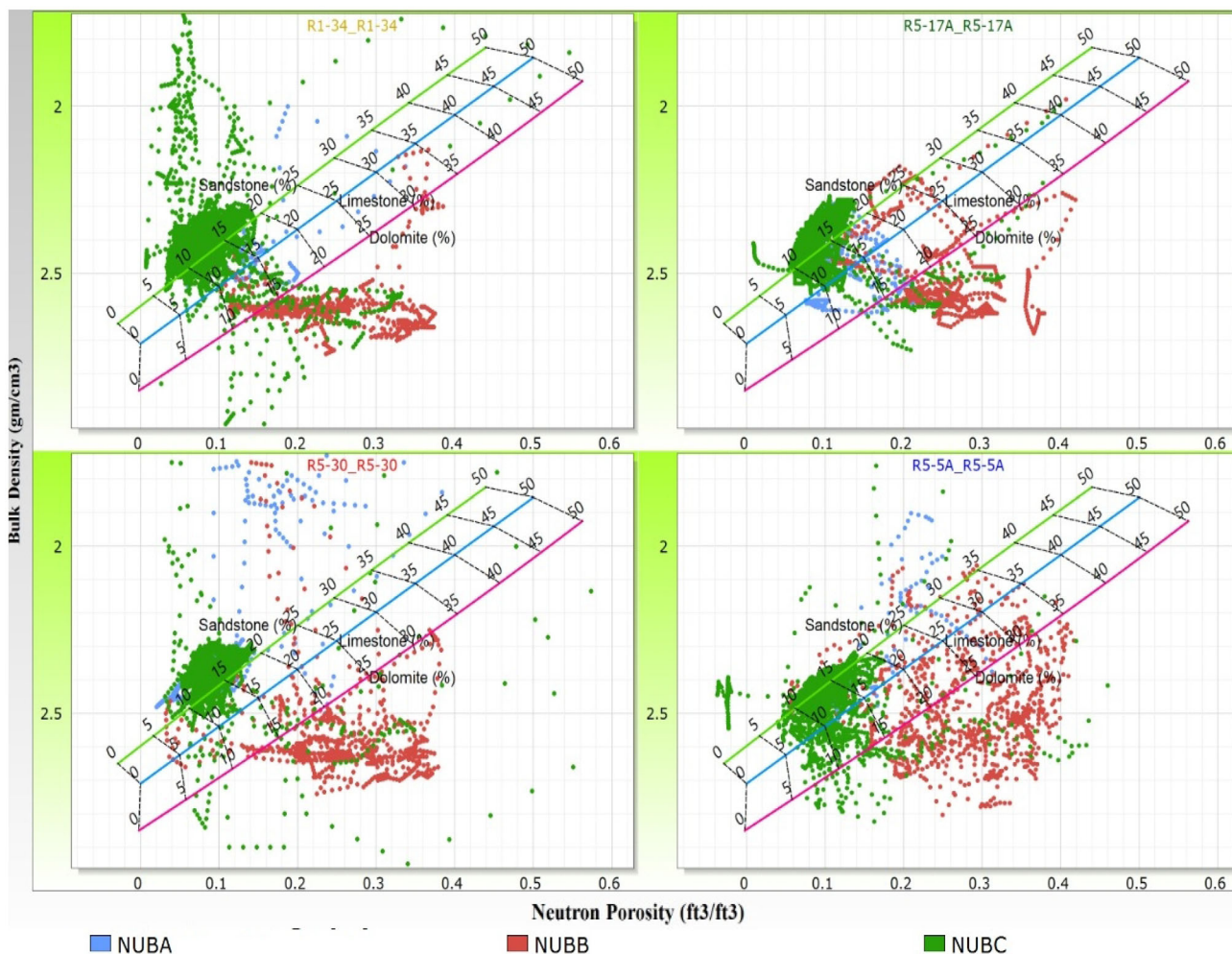
Fig. 5 Neutron–density cross-plots illustrating the matrix composition of the Nubian A, B, and C members in Ramadan oil field wells, Central Gulf of Suez, Egypt
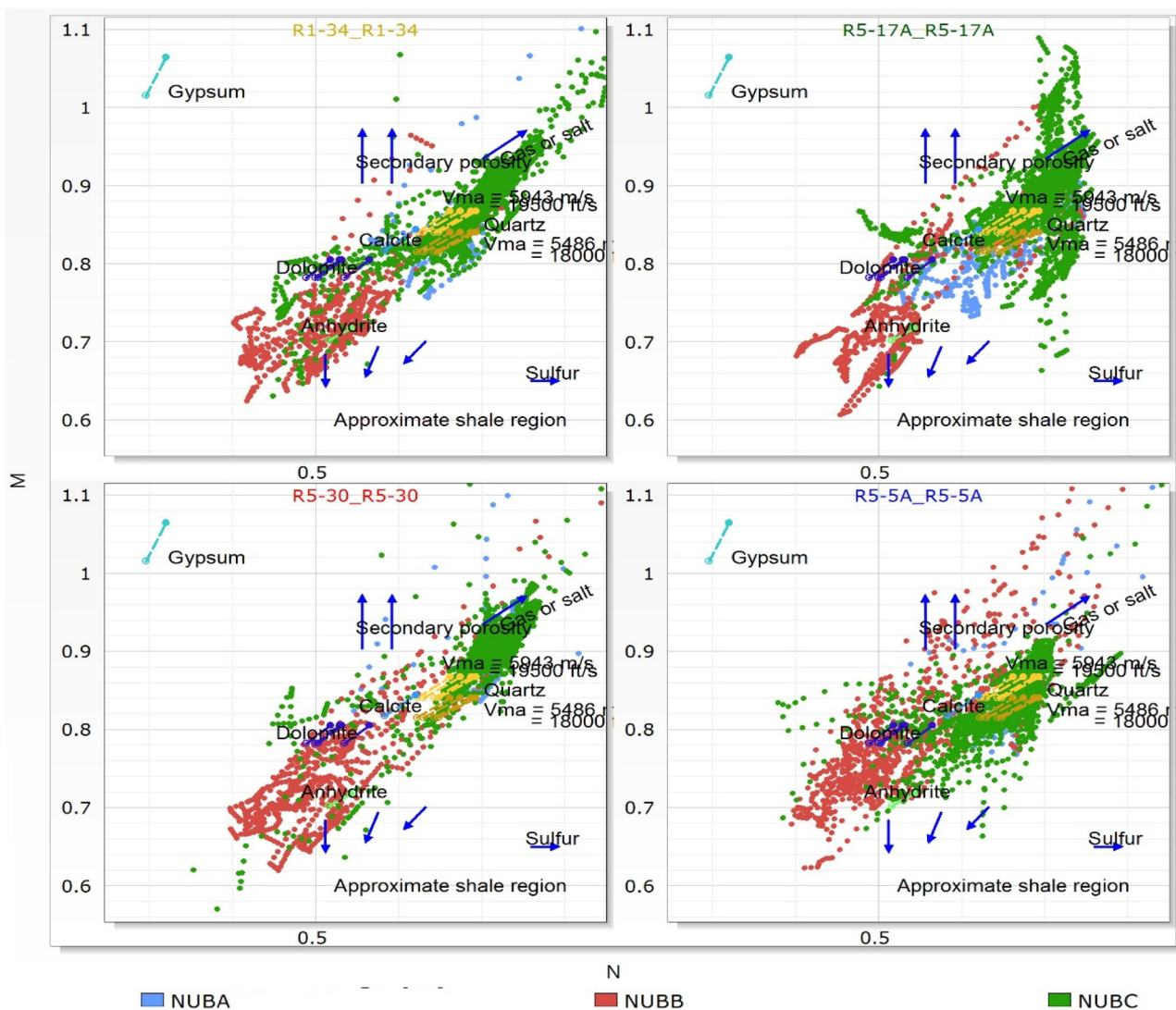
Fig. 6 M–N cross-plots typifying the lithologic properties of the Nubian A, B, and C members in Ramadan oil field wells, Central Gulf of Suez, Egypt

in the Nubian A, and B members (Table 1). In order to investigate the lateral variation of these parameters in the studied field, a set of isoparametric maps were plotted. The Nubian C member presents the main reservoir target in the Ramadan oil field with a net-pay thickness greater than 122 m (Table 1). The net-pay thickness increases northeast with a maximum thickness of 310 ft in the R5-17A well (Fig. 7A). Similarly, the shale volume distribution map shows that the lowest values are reported in the northeast in R5-17A well, whereas greater shale volume values are observed in the south and southeast where the Nubian C pay zone is thinning (Fig. 7B). Moreover, the water saturation distribution map illustrates an increasing trend in toward the north and south, whereas the lowest values (< 10%) are reported in the east and northeast at R5-17A well (Fig. 7C). Thus, the highest values of hydrocarbon saturation are observed in the eastern part of

the study region where the net-pay thickness increases and water saturation, shale volume decrease (Fig. 7D).

The Nubian B reservoir rocks host a relatively thin net-pay thickness (< 6 m) (Table 1), however, the net-pay thickness increases eastward in the R5-17A well (Fig. 8A). The Nubian B reservoir rocks in the eastern part of the study region display the lowest contents of shale volume, whereas the shale volume increases in the south and southwestern parts where the pay zone is thinning (Fig. 8B). Similar to Nubian B, the net-pay thickness of Nubian A increases eastward and northwestward (Fig. 8C). Additionally, the shale volume of Nubian A rocks decreases eastward with a minimum shale volume of 8.1% in the R5-17A well (Fig. 8D).
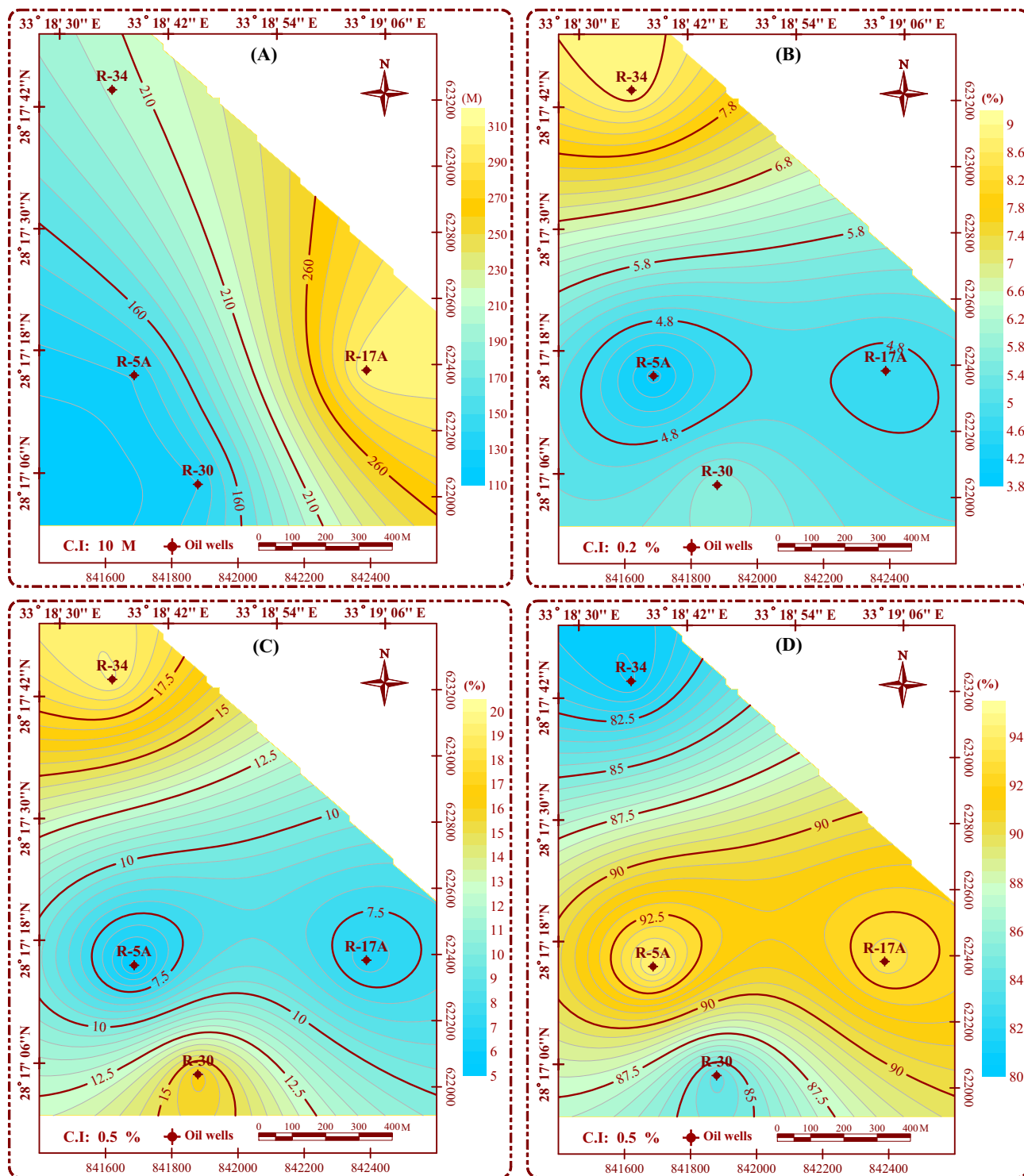
Fig. 7 Isoparametric maps for different petrophysical parameters in the Nubian C sediments illustrating the lateral distribution of (**A**) net-pay thickness, (**B**) shale volume, (**C**) water saturation and (**D**) hydrocarbon saturation in the studied Ramadan field wells
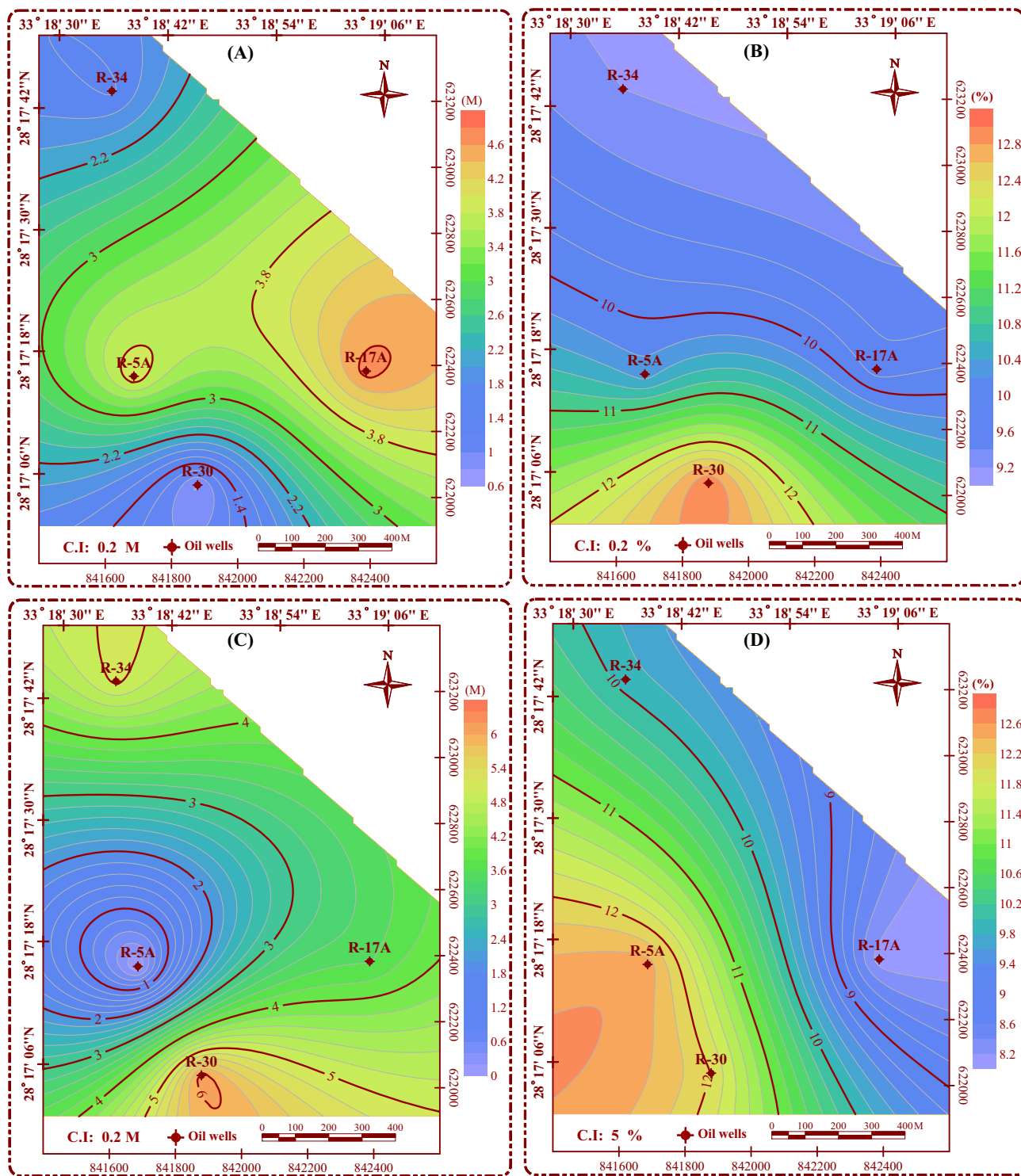
Fig. 8 Isoparametric maps illustrating the lateral distribution of net-pay thickness and shale volume in Nubian B (**A**, **B**) and A (**C**, **D**) members in the studied Ramadan field wells

4.3 Core Analysis of Nubian C Sandstone

Porosity, permeability, water saturation and grain density measurements of the core samples retrieved from Nubian C member in the R1-34 well revealed its excellent reservoir characteristics (Table 2). The helium porosity values range from 8.65 to 17.6% (mean = 12.77%, standard deviation = 2.53) (Fig. 9A). The horizontal permeability values are in the range of 0.26 md to 796 md, while the vertical permeability varies from 0.21 md and 427 md. The mean values of horizontal and vertical permeability are 96.55 md and 51.11 md, respectively, while the standard deviation for the horizontal and vertical permeability values are 173.61 md and 95.24 md, respectively (Fig. 9B, C). Thus, the relatively elevated standard deviation values reflect the reservoir heterogeneity with a wide degree of permeability anisotropy. On the other hand, the grain density values range from 2.63 and 2.66 g/cm^3 with mean values of 2.65 and a standard deviation of 0.007 (Fig. 9D), pointing to the uniform lithologic characteristics of the Nubian C reservoir rocks with a dominant quartzose sandstone composition.

## 4.4 Pore System Characteristics of the Nubian C Reservoir

Nubian C sandstones have wide range of porosity and permeability values reservoir approximately 60% of the Nubian sandstones having permeability values greater than 250 md. Positive correlations are observed between helium porosity (ϕ) and both horizontal permeability (Kh), and vertical (Kv) permeabilities with correlation coefficient values of 0.75 and 0.71, respectively. Additionally, linear regression relationships are observed between ϕ, Kh, and Kv by which the permeability values can be calculated as a function of porosity as follows:

$$K_h = 0.0113e^{0.6089\phi}$$

Table 2 Descriptive statistical analysis for vertical, horizontal permeability and helium porosity for Nubia C member in R1-34 well

Descriptive statistics	Permeability		Helium porosity (%)
	Vertical (md)	Horizontal (md)	
Mean	51.11	96.56	12.77
Standard error	13.34	24.31	0.35
Median	12.00	30.00	12.80
Mode	11.00	16.00	14.80
Standard deviation	95.24	173.61	2.53
Sample variance	9071.47	30,141.12	6.41
Kurtosis	7.91	8.26	−0.74
Skewness	2.79	2.88	0.14
Range	426.79	795.74	8.95
Minimum	0.21	0.26	8.65
Maximum	427.00	796.00	17.60

Fig. 9 Histograms and Trend lines curves for the measured helium porosity, horizontal and vertical permeability as well as grain density values in Nubian C sediments in R1-34 well of Ramadan oil field, Central Gulf of Suez, Egypt

Fig. 10 3D reservoir slicing illustrating the distribution of shale volume (**A**) and net pay (**B**) in the Nubian reservoir sediments

(A)

(B)
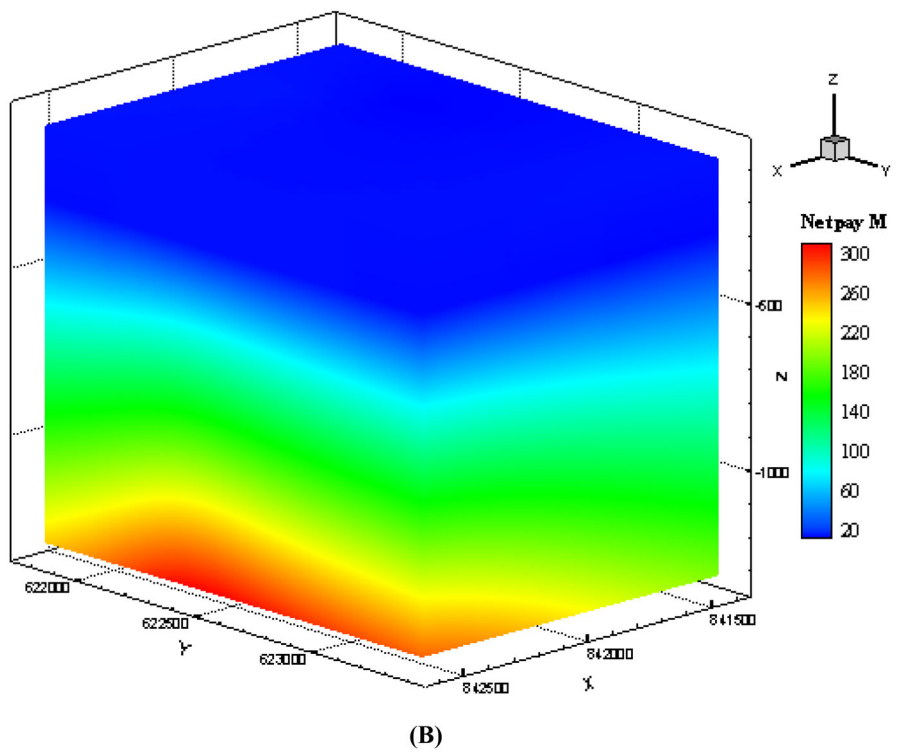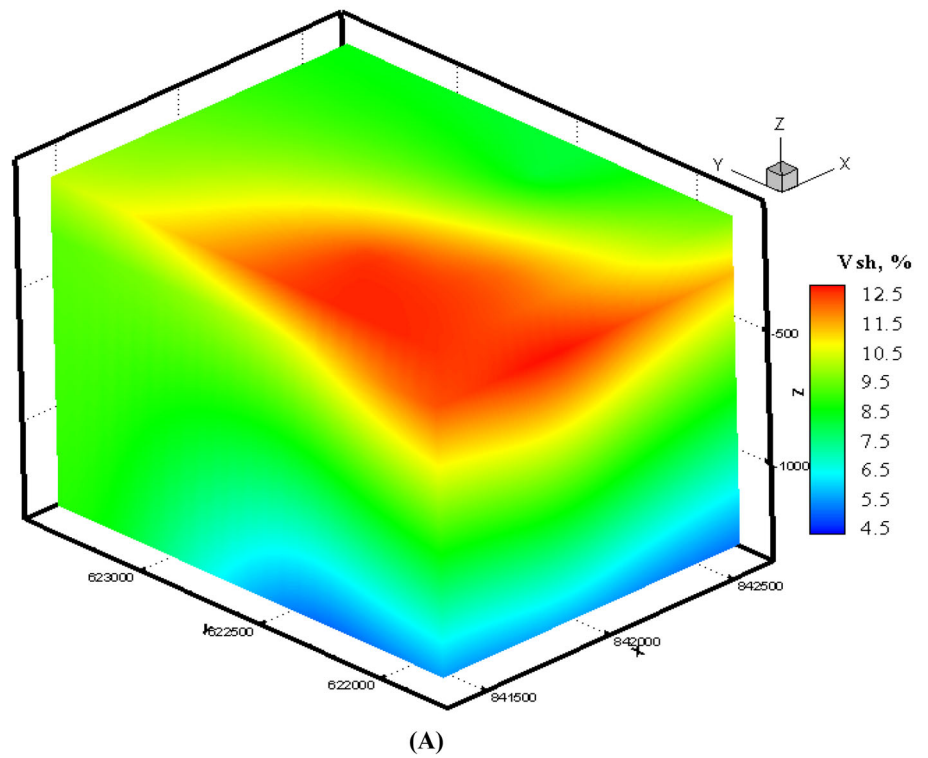
$$K_v = 0.0044e^{0.6196\phi}$$

Both vertical and horizontal permeability are positively correlated with a correlation coefficient of 0.88 and a linear regression equation as follows:

$$K_v = 0.4748\,K_h^{0.9806}$$

4.5 Reservoir Tomography (3D Slicing)

The 3D visualization of the shale volume typifies an upward increase in the shale content from Nubian C to Nubian A members. Moreover, the lowest shale content coincides with the bottom eastern part of the Nubian reservoir coinciding with the distribution of the Nubian C sandstone (Fig. 10A). On the other hand, the greatest content of shale occurs in the eastern uppermost part of the Nubian succession where the Nubian A and B rocks are enriched in clays. Similar to shale volume, the net-pay thickness decreases gradually upward and the greatest net-pay thicknesses occur at the bottom of the Nubian succession. The greatest values of net-pay thickness occur in the eastern lowermost part of the 3D reservoir block coinciding with Nubian C sandstone (Fig. 10B). Notably, the net-pay thickness is consistent with minimal contents of shale volume. Additionally, the net pay is thinning in the uppermost part of the Nubian succession where the shale volume increases in the Nubian A and B rocks.

5 Discussion

5.1 Reservoir Rock Typing (RRT)

The quality of the reservoir facies is mostly dependent on their porosity–permeability characteristics which infer on the pore system connectivity and heterogeneity [3–6, 8–10, 52–54]. The measured porosity and permeability values likely inherited from the presence of several reservoir rock types (RRT) with variable pore system characteristics. Furthermore, the 3D visualization of different petrophysical parameters within the studied Nubian reservoirs confirms existence of variable reservoir rock types, thus linking RRT distribution with the 3D reservoir slices which would enhance the predictability of potential reservoir facies, hence minimizing the exploration risks [55, 56]. RRT analysis encompasses the subdivision of reservoir facies into different rock types based on their pore geometry, structure, and connectivity as the main controlling factors on the reservoir storage and flow capacities [1, 3, 57–59]. Accurate determination of the different RRT and their distribution within the
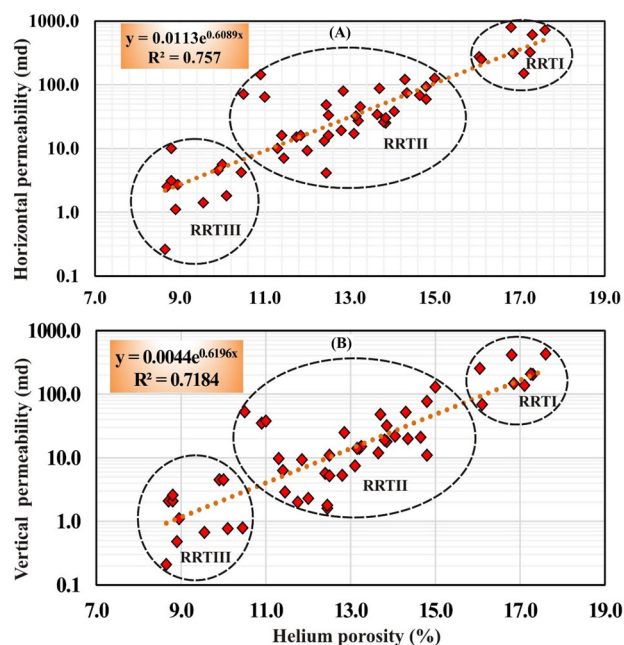

Fig. 11 Helium porosity versus horizontal (**A**) and vertical permeability (**B**) illustrating the poro-perm properties and different reservoir rock types (RRT) in the cored interval of Nubian C sediments in the Ramadan oil field

reservoir is elemental for understanding the reservoir dynamics, which aids in minimizing the exploration uncertainties and risks. Three different reservoir rock types have been discriminated in the cored interval of the Nubian C succession. RRTI constitutes the reservoir rocks having porosity values greater than 15% and horizontal and vertical permeability values higher than 100 md (Fig. 11A, B). RRTII comprises the Nubian C facies with porosity values between 10 and 15% and a wide permeability range between 100 and 1 md. On the other hand, the rocks with porosity values less than 10% and permeability less than 10 md are classified as RRTIII. Notably, wide heterogeneities in porosity and permeability values are observed in RRTII and RRTIII rocks reflecting their heterogeneous poro-perm characteristics. This is further confirmed by the deviation of the RRTII and RRTIII samples from the isotropic permeability line, whereas those of RRTI are plotted near the isotropic permeability line (Fig. 12). Thus, a minimal degree of pore network heterogeneity is observed in RRTI rocks, and therefore, they have the best reservoir characteristics. Moreover, directional pore network with $K_h > K_v$ is more common in the RRTII and RRTIII; thus, the fluids in these facies would flow horizontally rather than vertically. Reservoir rocks with directional permeability where the pore channels are oriented horizontally are often enriched in laminated clays and/or mica minerals, which are detrimental to the pore connectivity [4, 5, 60–62].

A strong correlation is observed between the reservoir quality parameters (e.g., shale volume, RQI, FZI, and R_{35})
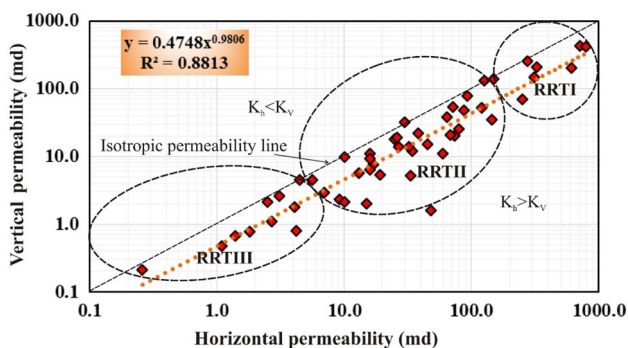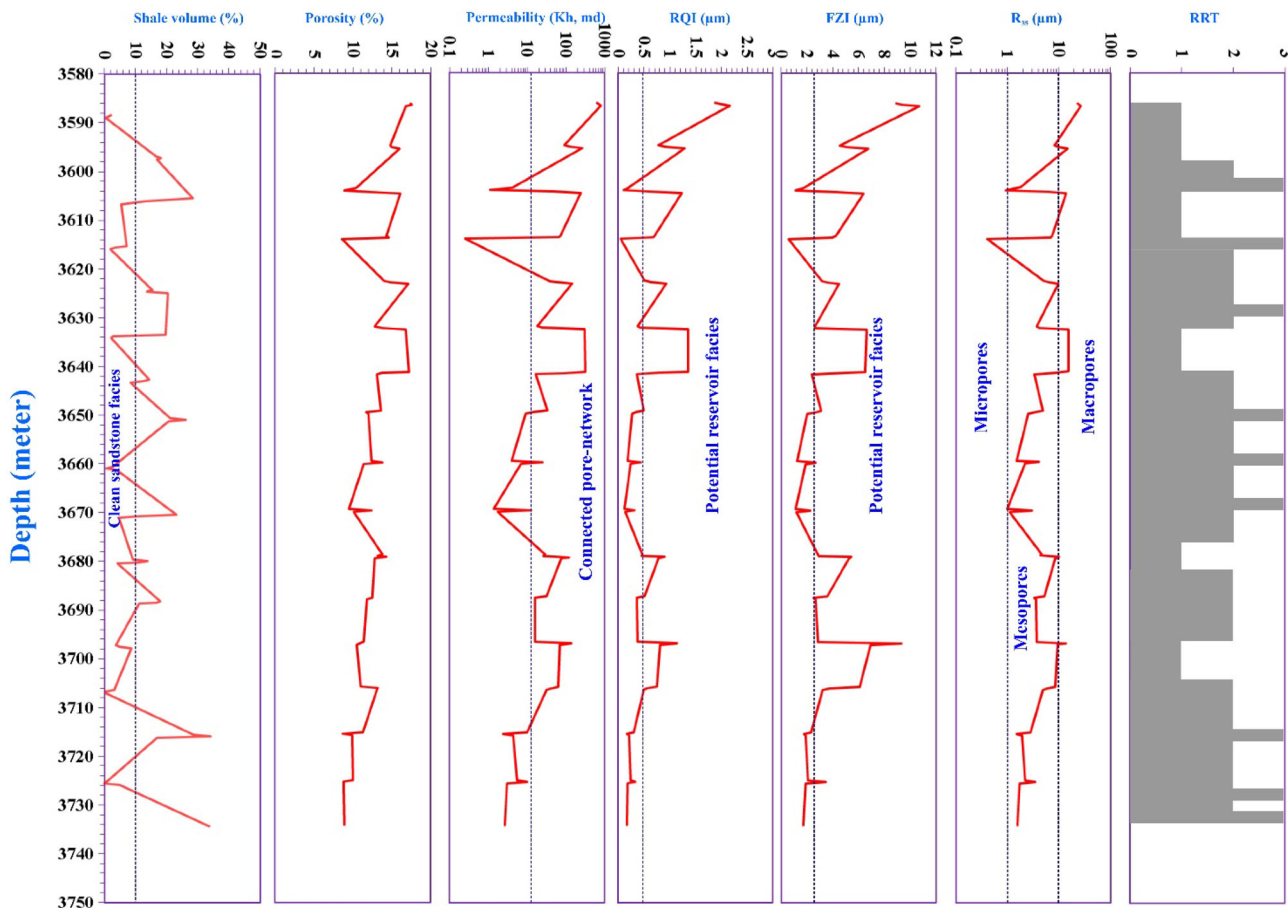
Fig. 12 Horizontal and vertical permeability cross-plot showing the pore connectivity characteristics of the different reservoir rock types in Nubian C sediments

and relatively lower RQI and FZI values than those in RRTI suggesting a more heterogeneous pore system. However, RRTII reservoir rocks contain both mesopores and macropores, but the mesopores are more common. Notably, the transition from RRTI to RRTIII is often corroborated with an increase in the shale volume, a decrease in pore connectivity, and pore throat radius. Therefore, we hypothesize that the shale volume induces a paramount control on the storage, flow capacities, and hence the overall reservoir quality of the Nubian C reservoir rocks in the Ramadan oil field. This explains the fluid flow behavior within the Nubian C reservoir as revealed from the 3D-reservoir slicing where the highest hydrocarbon saturation and net-pay thickness are always coinciding with the sandstone facies with minimal content of shale.

5.2 Capillary Properties and Impact of Confining Pressure on the Nubian C RRT

Mercury injection capillary pressure (MICP) results are sensitive to the variation in pore geometry and pore system

and the different reservoir rock types RRT (Fig. 13). The RRTI rocks have shale volume of less than 10%, and RQI, FZI values greater than 0.5 and 2, respectively. They are characterized by a well-connected pore network dominated by macropores. The RRTII and RRTIII reservoir rocks display a wide range of shale volume between 10 and 30%

Fig. 13 Vertical distribution of the different reservoir quality parameters illustrating the petrophysical characteristics of the different reservoir rock types RRT encountered in the cored interval of Nubian C sediments in R1-34 well

Fig. 14 Mercury pressure versus saturation cross-plot illustrating the capillary properties of the Nubian C RRTs in the Ramadan oil field
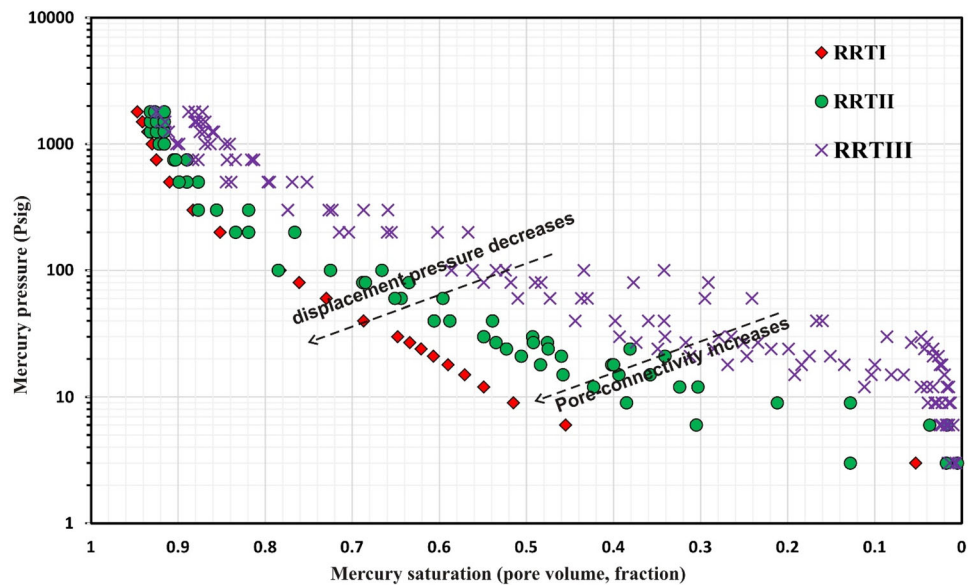

connectivity network as well as the pore water properties [3, 50, 63]. The morphology of the MCIP curves is influenced by the pore throat size, distribution, pore system network as well as the pore water type and content. The MCIP curves reveal a wide variation in the pore system characteristics of the Nubian C reservoir rock types. On the mercury pressure versus mercury saturation plot (Fig. 14), RRTI reservoir rocks display distinctive curves characterized by the lowest displacement pressure values (~ 10 psi air/mercury), and the mercury saturation values increase progressively with increasing the injection pressure typifying that the mercury can displace water easily in the pore system. On the other hand, the displacement pressure values are relatively higher in RRTII and RRTIII reservoir rocks with values ranging from 10 to 100 psi air/mercury. The morphology of the curves and the wide variation in the displacement pressure values basically reflect the pore structure, size, and connectivity. Large and well-connected pores become readily saturated with mercury at the lowest values of injection pressure [64]. Moreover, the occurrence of dead-end pores would increase the displacement pressure values as they are often saturated with irreducible water that could not be displaced [3, 50, 65, 66]. Thus, we hypothesize that the RRTI facies have a well-connected pore network dominated by macropores with minimal contents of dead-ends and irreducible water. In contrast, the content of dead-ends increases and the degree of pore connectivity decreases from RRTI to RRTIII.

The impact of confining pressure on the porosity of the Nubian C rock types increases from RRTI to RRTIII rocks. RRTI sandstones display almost flat curves on the porosity versus overburden pressure cross-plots typifying a minimal volume of pore reduction due to incremental increase of pressure from 500 to 6000 psi (Fig. 15A). Thus, the RRTI

sandstones are the most resistant to porosity reduction up on compaction. The porosity reduction (PRØ) in RRTI rock due to overburden pressure is in the range of 2.5 and 4%. The impact of overburden pressure on the pore volume is also mild in RRTII rocks displaying also flat curves where the porosity reduction values range from 2.8 and 5.5%. On the other side, the impact of overburden pressure and compaction is more significant in RRTIII rocks which display relatively steeper curves with an abrupt decrease in porosity by more than 10% up on increasing the overburden pressure from 500 to 1000 psi. The porosity reduction in RRTIII reservoir rocks is in the range of 4 and 10%. Similarly, the permeability reduction (PR_{Kh}) due to overburden pressure is more pronounced in the RRTIII than in RRTI and RRTII. RRTI and RRTII sandstones display flat curves with PR_{Kh} values ranging between 5 and 9% (Fig. 15B).

On the other hand, the PR_{Kh} in RRTIII reservoir rocks reaches up to 30%. Thus, the reduction of the pore throat and obstruction of pore connectivity up on compaction is more prominent in RRTIII reservoir rocks than that in RRTI and RRTII facies. These wide variations in compressibility of the different RRTs are related to their compositional characteristics. The quartzose composition of RRTI sandstones dominated by rigid quartz grains supports the facies framework strength against compaction and pore reduction. On the other side, the enrichment of shale in RRTIII reservoir rocks is detrimental to the framework strength against compaction as the clays and ductile argillaceous materials are squeezed in the pore spaces, resulting in a significant decrease in porosity and permeability upon compaction [10, 67, 68]. Therefore, we hypothesize that RRTI and RRTII sandstones have a better potentiality for primary porosity preservation and hence

Fig. 15 Overburden pressure versus porosity (**A**) and permeability (**B**) illustrating the impact of compaction on the pore volume and pore network connectivity in the Nubian C sediments
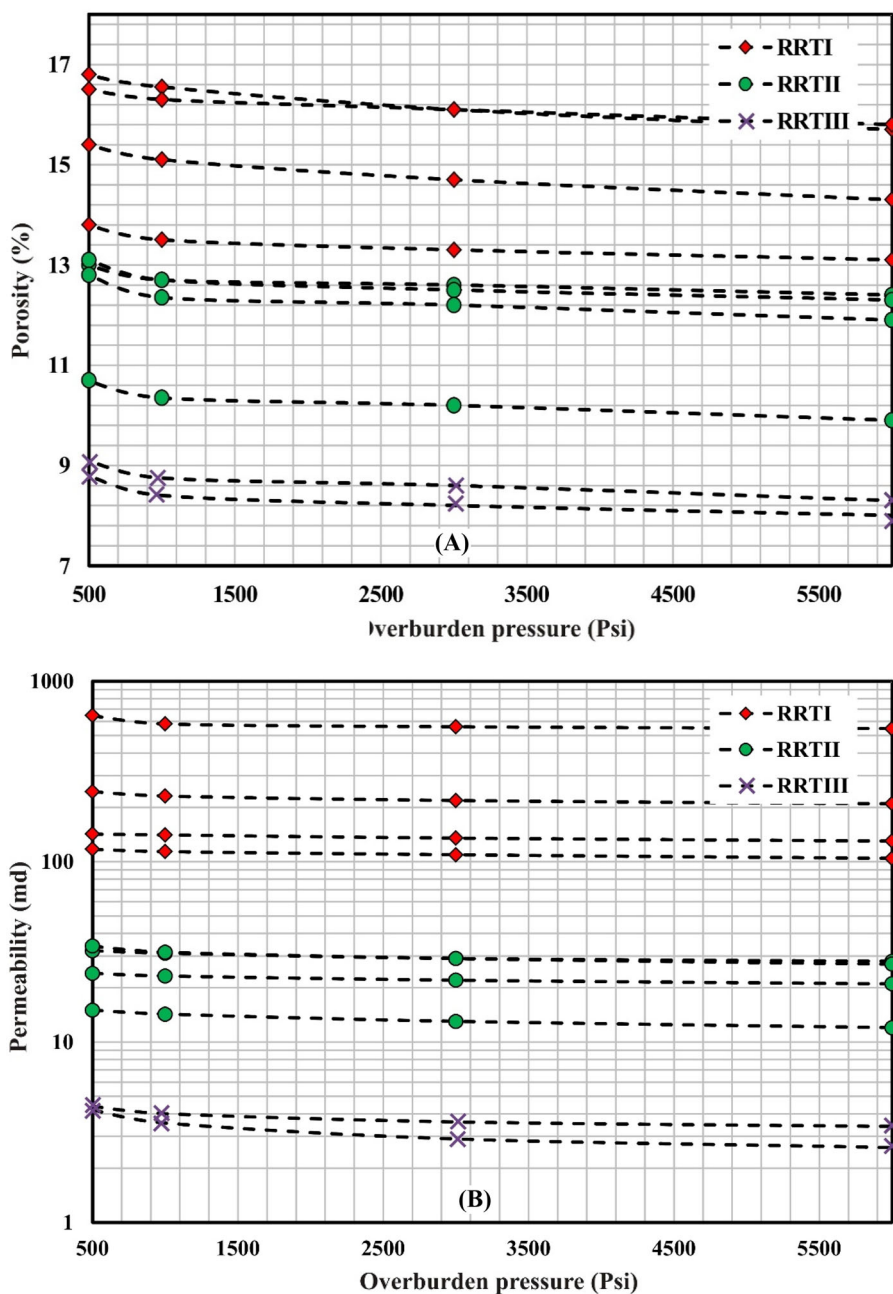
they will not lose their excellent storage and flow capacities even at great burial depths.

5.3 Implications for Reservoir Performance and Field Development

Detailed understanding of the factors controlling the spatial distribution of the best reservoir facies and the associated RRT is crucial for reservoir exploration and development strategies [1–3]. Furthermore, understanding the link between the compositional attributes and reservoir flow

dynamics will aid in improving the reservoir facies predictability and minimizing the exploration risks [67, 68]. Petrophysical results and 3D reservoir slices as well as the isoparametric maps reveal that the best reservoir is associated with quartzose sandstone facies having minimal content of clays and carbonate cements. These facies are classified as RRTI and RRTII sandstone units. These units are the main fluid flow conduits within the Nubian sandstone reservoir. The connectivity of RRTI and RRTII sandstones likely increases in the eastern part of the studied field where a minimal content of clay volume has been reported. Thus, we

interpret the enhanced reservoir performance in the eastern part of the study region to the relative thickening of RRTI, RRTII sandstones. On the other hand, occurrence of the clay-rich facies associated with RRTIII rocks would reduce the reservoir connectivity and hence the reservoir performance.

6 Conclusions

The reservoir characteristics of the pre-Cenomanian Nubian succession in the Ramadan oil field, Gulf of Suez, were investigated based on comprehensive integration between wireline logs and core data. The pre-Cenomanian clastics are charged from several reservoir levels (e.g., Duwi limestone), however, the thickness and distribution of pay zones are mainly controlled by their reservoir properties and pore system characteristics. The Nubian reservoir rocks comprise a thick siliciclastic succession of sandstones, siltstones, and shales of the Nubian C, B, and A members. The sand/shale ratio decreased from Nubian C to A and B. The reservoir quality varies greatly among the Nubian members where thick intervals of net-pay > 122 m are restricted to the Nubian C sandstones, whereas the other Nubian members host thin pay zones < 15 m.

3D reservoir slicing illustrates that good reservoir facies with the greatest net-pay thicknesses and lowest contents of shale are restricted to the southeastern parts of the study region. The Nubian C rocks are classified into three main reservoir rock types (RRT). RRTI and RRTII facies have the best reservoir characteristics with well-connected pore systems dominated by macropores. On the other hand, RRTIII facies are clay-rich and therefore have relatively lower porosity and permeability values. RRTI and RRTII reservoir rocks have the best capillary properties with the lowest values of displacement pressure (< 10 psi), whereas the RRTIII have relatively higher displacement pressure values due to abundant dead-ends infilled with irreducible fluids. These rocks are more resistant to compaction than the RRTIII, and therefore, they have more potential for primary porosity and permeability preservation.

Declarations

Conflict of interest The authors want to declare that they do not have any conflict of interests to disclose.

References

1. Guo, Q.; Wang, Y.; Gao, X.; Ma, T.: A new model (DRARCH) for assessing groundwater vulnerability to arsenic contamination at basin scale: a case study in Taiyuan basin, northern China. Environ. Geol. **52**(5), 923–932 (2007)
2. Skalinski, M.; Kenter, J.: Carbonate petrophysical rock typing: integrating geological attributes and petrophysical properties while linking with dynamic behaviour. Geol. Soc. **406**, 229–259 (2014). https://doi.org/10.1144/SP406.6
3. El Adl, H.; Leila, M.; Ahmed, M.A.; Anan, T.; El- Shahat, A.: Integrated sedimentological and petrophysical rock-typing of the Messinian Abu Madi formation in South Batra gas field, onshore Nile Delta, Egypt. Mar. Petrol. Geol. **124**, 1–28 (2021)
4. Leila, M.; El-Sheikh, I.; Abdelmaksoud, A.; Radwan, A.A.: Seismic sequence stratigraphy and depositional evolution of the Cretaceous-Paleogene sedimentary successions in the offshore Taranaki Basin, New Zealand: implications for hydrocarbon exploration. Mar. Geophys. Res. **43**, 23 (2022). https://doi.org/10.1007/s11001-022-09483-z
5. Leila, M.; Yasser, A.; El Bastawesy, M.; El Mahmoudi, A.: Seismic stratigraphy, sedimentary facies analysis and reservoir characteristics of the Middle Jurassic syn-rift rocks in Salam Oil Field, north Western Desert, Egypt. Mar. Petrol. Geol. (2022). https://doi.org/10.1016/j.marpetgeo.2021.105466
6. Amaefule, J. O.; Altunbay. M.; Tiab, D.; Kersey, D. G. and Keelan, D. K.: Enhanced reservoir description: using core and log data to identify hydraulic (flow) units and predict permeability in uncored intervals/wells. In: The 68th annual technical conference and exhibition of the society of petroleum engineers, Houston, Texas, 3–6 Oct 1993, pp. 205–220
7. Jardim, C.M.; De Ros, L.F.; Ketzer, J.M.: Reservoir quality assessment and petrofacies of the lower cretaceous siliciclastic, carbonate and hybrid arenites from the Jequitinhonha Basin, Eastern Brazil. J. Pet. Geol. **34**(3), 305–335 (2011). https://doi.org/10.1111/j.1747-5457.2011.00507.x
8. Nabawy, B.S.; Basal, A.M.K.; Sarhan, M.A.; Safa, M.G.: Reservoir zonation, rock typing and compartmentalization of the Tortonian-Serravallian sequence, Temsah Gas Field, offshore Nile Delta, Egypt. Mar. Pet. Geol. **92**, 609–631 (2018)
9. Leila, M.; Mohamed, A.: Diagenesis and petrophysical characteristics of the shallow Pliocene sandstone reservoirs in the Shinfas Gas Field, onshore Nile Delta, Egypt. J. Petrol. Explor. Prod. Technol. **10**, 1–19 (2020)
10. Leila, M.; Ali, E.; Abu El-Magd, A.; AlWaan, L.; Elgendy, A.: Formation evaluation and reservoir characteristics of the Messinian Abu Madi sandstones in Faraskour gas field, onshore Nile delta, Egypt. J. Petrol. Explorat. Product. Technol. **11**, 133–155 (2021). https://doi.org/10.1007/s13202-020-01011-2

11. Radwan, A. E.; Wood, D. A.; Mahmoud, M. and Tariq, Z.: Gas adsorption and reserve estimation for conventional and unconventional gas resources. In D. A. Wood & J. Cai (Eds.), Sustainable geoscience for natural gas sub-surface systems, Elsevier, pp. 345–382 (2022) https://doi.org/10.1016/B978-0-323-85465-8.00004-2

12. Radwan, A.E.; Nabawy, B.; Kassem, A.; Hussein, W.: Implementation of rock typing on waterflooding process during secondary recovery in oil reservoirs: a case study, El Morgan Oil Field, Gulf of Suez, Egypt. Nat. Resour. Res. **30**, 1667–1696 (2021). https://doi.org/10.1007/s11053-020-09806-0

13. Radwan, A.E.; Wood, D.; Abudeif, A.; Attia, M.; Mahmoud, M.; Kassem, A.; Kania, M.: Reservoir formation damage; reasons and mitigation: a case study of the Cambrian-Ordovician Nubian 'C' sandstone gas and oil reservoir from the Gulf of Suez Rift Basin. Arab. J. Sci. Eng. **47**, 11279–11296 (2022). https://doi.org/10.1007/s13369-021-06005-8

14. Abdine, A.S.; Meshref, W.; Shahin, A.N.;Garissino, R.; Shazly, S.: Ramadan field I Egypt: Gulf of Suez basin. In: S.M. Landon (Ed.), Interior Rift Basins. AAPG Memoir 58, pp. 97–122 (1994)

15. El Diasty, W.S.; El Beialy, S.Y.; Mostafa, A.R.; Peters, K.: Chemometric differentiation of oil families and their potential source rocks in the Gulf of Suez. Nat. Resour. Res. **29**, 2063–2102 (2020). https://doi.org/10.1007/s11053-019-09569-3

16. Barakat, M.G.: General Review of the Petroliferous Provinces of Egypt. Petroleum and Gas Project, Cairo Univ./M.I.T. Technology Planning Program (1982)

17. Zahran, M. E.; Meshref, W.: The Northern Gulf of Suez Basin Evolution, Stratigraphy and Facies Relationship. Proceedings of the 9th Petroleum Exploration and Production Seminar, Egypt, v. 1, pp. 110–126 (1988)

18. Mostafa, A. R.: Organic geochemistry of source rocks and related crude oils in the Gulf of Suez. Egypt. Berliner Geowissenschaftliche Abhandlungen, A, 147, 163 (1993)

19. Alsharhan, A.S.; Salah, M.G.: Geology and hydrocarbon habitat in a rift setting: northern and central Gulf of Suez, Egypt. Can. Petrol. Geol. Bull. **43**(2), 156–176 (1995)

20. Nabawy, B.S.; Rochette, P.; Géraud, Y.: Electric pore fabric of the Nubia sandstones in south Egypt: characterization and modelling. Geophys. J. Int. **183**(2), 681–694 (2010). https://doi.org/10.1111/j.1365-246X.2010.04789.x

21. El Gendy, N.; Barakat, M.; Abdallah, H.: Reservoir assessment of the Nubian sandstone reservoir in South Central Gulf of Suez, Egypt. J. Afr. Earth Sci. **129**, 596–609 (2017). https://doi.org/10.1016/j.jafrearsci.2017.02.010

22. Schlumberger: Well Evaluation Conference, pp. 1–64 (1984)

23. Alsharhan, A.S.: Petroleum geology and potential hydrocarbon plays in the Gulf of Suez rift basin, Egypt. AAPG Bull. **87**(1), 143–180 (2003)

24. El Diasty, W.S.; Peters, K.E.: Genetic classification of oil families in the central and southern sectors of the Gulf of Suez, Egypt. J. Petrol. Geol. **37**, 105–126 (2014)

25. Pivnik, D.A.; Ramzy, M.; Steer, B.L.; Thorseth, J.; El Sisi, Z.; Gaafar, I.; Tucker, R.S.: Episodic growth of normal faults as recorded by syntectonic rocks, July oil field, Suez rift, Egypt. AAPG Bull. **87**(6), 1015–1030 (2003). https://doi.org/10.1306/02050301100

26. Richardson, M.; Arthur, M.A.: The Gulf of Suez northern Red Sea Neogene rift: a quantitative basin analysis. Mar. Pet. Geol. **5**(3), 247–270 (1988)

27. Moustafa, A.R.: Controls on the geometry of transfer zones in the Suez rift and northwest Red Sea: implications for the structural geometry of rift systems. AAPG Bull. **86**(6), 979–1002 (2002)

28. Dancer, P. N.; Collins, J.;Beckly, A.; Johnson, K.; Campbell, G.; Mumaw, G. and Hepworth, B.: Exploring subtle exploration plays in the Gulf of Suez. In Geological Society, London, Petroleum Geology Conference series. Geological Society of London, Vol. 7, No. 1, pp. 771–781, (2010). https://doi.org/10.1144/0070771

29. Plaziat, J. C.; Montenat, C.; Barrjer, P.; Janin, M. C.; Orszag-Sperber, F. and Philobbos, E. R.: Stratigraphy of the Egyptian syn-rift deposits: correlations between axial and peripheral sequences of the north-western Red Sea and Gulf of Suez and their relations with tectonics and eustasy. In: Purser BH, Bosene DWJ (eds) Sedimentation and tectonics in rift basins Red Sea-Gulf or Aden. Chapman & Hall, London, pp. 211–222 (1998). https://doi.org/10.1007/978-94-011-4930-3_13

30. El Nady, M.M.; Ramadan, F.S.; El Hemimey, W.A.; Saleh, A.H.: Lithofacies characterization and source rock assessment of the lower-middle Miocene Successions in the northern part of Ramadan oil field, central Gulf of Suez, Egypt. Arab. J. Geosci. **15**, 634 (2022). https://doi.org/10.1007/s12517-022-09791-z

31. Bosworth, W. and McClay, K.: Structural and stratigraphic evolution of the Gulf of Suez rift, Egypt: A synthesis. In P. A. Ziegler, W. Cavazza, A. H. F. Robertson, & S. CrasquinSoleau (Eds.), Peri-Tethys Memoir 6: Peri-Tethyan Rift/ Wrench Basins and Passive Margins (. Paris: Memoires du Muse ´um National dHistoire Naturelle de Paris, Vol. 186, pp. 567–606 (2001)

32. Soliman, A.E.; El Nahas, H.A.; Omran, A.A.: Geology of wadi Wassif area, central Eastern Desert, Egypt, with emphasis on mineralogy of stream rocks. Nucl. Sci. Sci. J. **1**(1), 85–97 (2012)

33. El-Ghali, M.A.K.; El Khoriby, E.; Mansurbeg, H.; Morad, S.; Ogle, N.: Distribution of carbonate cements within depositional facies and sequence stratigraphic framework of shoreface and deltaic arenites, Lower Miocene, the Gulf of Suez rift, Egypt. Mar. Petrol. Geol. **45**, 267–280 (2013). https://doi.org/10.1016/j.marpetgeo.2013.04.019

34. Pomeyrol, R.: Nubian sandstone: AAPG Bulletin, v. 52, no. 9, p. 589–600 (1968)

35. El Barkooky, A. N.: Stratigraphic framework of the Paleozoic in the Gulf of Suez region, Egypt, in Proceedings 1st Conference on Geology of Arab World, I, Egypt; pp. 1–19 (1992)

36. Darwish, M.; El-Araby, A.M.: Petrography and diagenetic aspects of some siliciclastic hydrocarbon reservoirs in relation to the rifting of the Gulf of Suez, Egypt. J. Geol. **3**, 1–25 (1994)

37. Said, R.: Explanation notes to accompany the geological map of Egypt. Egypt. Geol. Surv. **56**, 123 (1971)

38. Hassan, A. A.: A new Carboniferous occurrence in Abu Durba, Sinai, Egypt, in Proceedings of the 6th Arab Petroleum Congress, Baghdad, Vol. 2, pp. 1–8 (1967)

39. Alsharhan, A.S.; Salah, M.G.: A common source rock for Egyptian and Saudi hydrocarbons in the Red Sea. Am. Asso. Petrol. Geol. Bull. **81**(10), 1640–1659 (1997)

40. Abdallah, A.M.; Adindani, A.; Fahmy, N.: Stratigraphy of Upper Paleozoic rocks, Western side of the Gulf of Suez, Egypt. Egypt. Geol. Surv. **25**, 1–18 (1963)

41. Bosworth, W.: A high-strain rift model for the southern Gulf of Suez (Egypt). In J. J. Lambaise (Ed.), Hydrocarbon habitat in rift basins. London: Geological Society of London, Special Publication, Vol. 80, pp. 75–112 (1995)

42. Poupon, A.; Leveaux, J.: Evaluation of water saturation in shaly formations. In Proceedings of the SPWLA 12th annual logging symposium (1971)

43. Asquith, G. B.; Gibson, C. R.: Basic well log analysis for geologists. (Vol. 3),Tulsa: American Association of Petroleum Geologists (1982)

44. Schlumberger: Log interpretation manual/application. Vol. 2 Houston, Schlumberger well services, Inc., pp. 87 (1974)

45. Bruke, J. A.; Campbell, R. L.; Schmidt, A. W.: The litho-porosity cross plot. The log analyst (SPWLA) Vol. 10, No. 6 (1969)

46. Davis, J. C.: Statistics and data analysis in geology, John Wiley and Sons, New York, Vol. 646 (1986)

47. Dean, E.W.; Stark, D.D.: A convenient method for the determination of water in petroleum and other organic emulsions. Ind. Eng. Chem. **5**, 486–490 (1920). https://doi.org/10.1021/ie50125a025

48. Winland, H.D.: Oil Accumulation in Response to Pore Size Changes, Weyburn Field, Saskatchewan. Amoco Production Research Report F72-G-25 (1972)

49. Leverett, M.: Capillary behavior in porous solids. Trans. AIME **142**(01), 152–169 (1941). https://doi.org/10.2118/941152-G

50. Vavra, C.L.; Kaldi, J.G.; Sneider, R.M.: Geological applications of capillary pressure: a review. AAPG Bull. **76**(6), 840–850 (1992). https://doi.org/10.1306/BDFF88F8-1718-11D7-8645000102C1865D

51. Schlumberger: Well Evaluation Conf., Libya Surv. Tech. Schlumberger France. 96 p (1970)

52. Kim, J.; Yong, L.; Hisada, K.: Depositional and compositional controls on sandstone diagenesis, the Tetori Group (Middle Jurassic-Early Cretaceous), central Japan. Sedmint. Geol. **195**, 183–202 (2007)

53. Nabawy, B.S.; Rashed, M.A.; Mansour, A.S.; Afify, W.S.M.: Petrophysical and microfacies analysis as a tool for reservoir rock typing and modeling: Rudeis Formation, offshore october oil field, Sinai. Mar. Pet. Geol. **97**, 260–276 (2018)

54. Levorsen, A. I.: Geology of Petroleum. W. H. Freeman and San Francisco, U S A, 350 p. (1967)

55. Ghoneimi, A.: Reservoir 3D- Slicing of Lower Baharia pay zones in Hayat and Yaser oil fields, Western Desert, Egypt. J. Appl. Geophys. **1**, 129–142 (2002)

56. Al-Alfy, I.; El-Hawary, A.; Mohammad, H.; Shaheen, M.; Nabih, M.: 3D Slicing of weighted index for reservoir quality of lower Miocene Rocks, Belayim Marine Oil Field, Gulf of Suez. Egypt. J. Geosci. Environ. Protect. **10**, 55–65 (2022). https://doi.org/10.4236/gep.2022.108005

57. Pittman, E.D.: Relationship of porosity and permeability to various parameters derived from mercury injection-capillary pressure curves for sandstone. AAPG Bull. Am. Assoc. Petrol. Geol. **76**(2), 191–198 (1992)

58. Rushing, J. A.; Newsham, K. E.; Blasingame, T. A.: Rock typing: Keys to understanding productivity in tight gas sands. In SPE Unconventional Reservoirs Conference. OnePetro (2008). doi: https://doi.org/10.2118/114164-MS

59. Saleh, A.H.; Farag, A.E.; Eysa, E.A.: Reservoir quality of Abu Roash (G) member in Karama Oil Field, East Bahariya Concession, North Western Desert, Egypt. Arab. J. Geosci. (2021). https://doi.org/10.1007/s12517-020-06349-9

60. Ehrenberg, S.N.: Relationship between diagenesis and reservoir quality in sandstones of the Garn formation, Haltenbanken, Mid-Norwegian Continental Shelf. AAPG Bull. **74**(10), 1538–1558 (1990). https://doi.org/10.1306/0C9B2515-1710-11D7-8645000102C1865D

61. Walderhaug, O.; Eliassen, A.; Aase, N.E.: Prediction of permeability in quartz-rich sandstones: examples from the Norwegian Continental Shelf and the Fontainebleau Sandstone. J. Sediment. Res. **82**(12), 899–912 (2012). https://doi.org/10.2110/jsr.2012.79

62. Leila, M.: Clay minerals distribution in the pre-, syn-Messinian salinity crisis rocks of the onshore Nile Delta, Egypt: mineral origin and implications on the reservoir quality. J. Afr. Earth Sci. **154**, 35–48 (2019)

63. Kashif, M.; Cao, Y.; Yuan, G.; Asif, M.; Javed, K.; Mendez, J.N.; Khan, D.; Miruo, L.: Pore size distribution, their geometry and connectivity in deeply buried Paleogene Es1 sandstone reservoir, Nanpu Sag, East China. Pet. Sci. **16**, 981–1000 (2019). https://doi.org/10.1007/s12182-019-00375-3

64. Jennings, J.B.: Capillary pressure techniques: application to exploration and development geology. AAPG Bull. **71**(10), 1196–1209 (1987)

65. Leila, M.; Moscariello, A.: Depositional and petrophysical controls on the volumes of hydrocarbons trapped in the Messinian reservoirs, onshore Nile Delta, Egypt. Petroleum **4**, 250–267 (2018)

66. Yasser, A.; Leila, M.; El Bastawesy, M.; El Mahmoudi, A.: Reservoir heterogeneity analysis and flow unit characteristics of the Upper Cretaceous Bahariya Formation in Salam Field, north Western Desert, Egypt. Arab. J. Geosci. **14**, 1635 (2021). https://doi.org/10.1007/s12517-021-07985-5

67. Jonas, E.C.; McBride, E.F.: Diagenesis of sandstone and shale: application to exploration for hydrocarbons: continuing education program publication 1. University of Texas at Austin, Austin, Texas, Department of Geological Sciences (1977)

68. Leila, M.; Moscariello, A.; Segvic, B.: Geochemical constraints on the provenance and depositional environment of the Messinian rocks, onshore Nile Delta, Egypt: implications for the late Miocene paleogeography of the Mediterranean. J. Afr. Earth Sci. **143**, 215–241 (2018)